Solid Fluoride Electrolytes and Their Composite with Carbon: Issues and Challenges for Rechargeable Solid State Fluoride-Ion Batteries

Antonin Grenier, Ana-Gabriela Porras Gutierrez, Monique Body, Christophe Legein, Fabien Chretien, Encarnación Raymundo-Piñero, Mickaël Dollé, Henri Groult, Damien Dambournet

Article

Solid Fluoride Electrolytes and Their Composite with Carbon: Issues and Challenges for Rechargeable Solid State Fluoride-Ion Batteries

Antonin Grenier, Ana-Gabriela Porras Gutierrez, Monique Body, Christophe Legein, Fabien Chretien, Encarnacion Raymundo-Piñero, Mickael Dollé, Henri Groult, and Damien Dambournet

J. Phys. Chem. C, **Just Accepted Manuscript** • DOI: 10.1021/acs.jpcc.7b07988 • Publication Date (Web): 24 Oct 2017

Solid Fluoride Electrolytes and their Composite with Carbon: Issues and Challenges for Rechargeable Solid State Fluoride-Ion Batteries

Antonin Grenier,[†] *Ana Gabriela Porras-Gutierrez,*[†] *Monique Body,*[§] *Christophe Legein,*[§] *Fabien Chrétien,*[‡] *Encarnación Raymundo-Piñero,*[‡,∏] *Mickael Dollé,*[⊥] *Henri Groult,*[†] *and Damien Dambournet*[†,∏,*]

[†] Sorbonne Universités, UPMC Univ. Paris 06, CNRS, UMR 8234, PHENIX, F-75005 Paris, France

[§] Université Bretagne Loire, Université du Maine, UMR CNRS 6283, Institut des Molécules et des Matériaux du Mans (IMMM), Avenue Olivier Messiaen, 72085 Le Mans Cedex 9, France

[‡] CNRS, CEMHTI UPR3079, Univ. Orléans, F-4071 Orléans, France

[⊥] Département de Chimie, Université de Montréal C.P. 6128, succursale Centre-Ville Montréal, QC, H3C 3J7 Canada

[∏] Réseau sur le Stockage Electrochimique de l'Energie (RS2E), FR CNRS 3459, France

Abstract

Solid-state batteries relying on fluoride-ion shuttle are still at their early stage of development. Assessing the fluoride solid electrolyte's electrochemical stability and its conduction properties in a mixture with carbon, as well as the possible interaction of fluoride-ion with carbon both during the

electrode preparation and upon electrochemical reactions, are mandatory to enable future practical applications. Here, we discuss these points using LaF_3 doped with BaF_2 ($La_{0.95}Ba_{0.05}F_{2.95}$, LBF) as a benchmark solid fluoride electrolyte. We establish that lithium may be used as a pseudo-reference electrode to assess the electrochemical stability window of LBF and support the experiment with thermodynamic calculations. We demonstrate the chemical compatibility of LBF with carbon upon ball-milling, and investigate the electrical conductivity of the formed LBF-C composite. We use a LBF|LBF-C|LBF cell (in this configuration, LBF serves as electronically blocking electrode) to assess the ionic conductivity of the LBF-C composite. The results confirm that both electronic and ionic percolations are insured within the LBF-C composite despite a noticeable decrease of the ionic conductivity. Finally, we use a Li|LBF|LBF-C cell to evaluate the electrochemical fluorination of the carbon in the LBF-C composite. Our results suggest an electrochemical activity of carbon with fluoride ions. The possible interactions of carbon with fluorides to form insulating carbon fluoride (CF_x) must be considered when determining the operating voltage of FIBs.

Introduction

The electronegativity and low mass of fluorine make fluoride ion batteries (FIBs) promising candidates within the scope of developing new battery chemistries providing increased energy densities compared to conventional metal-ion batteries.[1] Anji Reddy and Fichtner were the first to provide a proof-of-concept of a rechargeable solid-state cell[2], raising the awareness of a conversion-based chemistry first proposed in the 1970s.[3–12] It was more recently demonstrated that fluoride ions could be reversibly intercalated in $LaSrMnO_4$[13], that CuF_2 was a reversible conversion cathode[14], and that oxyfluorides are possible conversion materials[15], further increasing the interest of the community for this chemistry.

Tysonite type (trigonal, *P*-3*c*1) solid solutions like $La_{1-x}Ba_xF_{3-x}$ (LBF) have been the focus of some research efforts with the purpose of understanding and increasing the fluoride conductivity to improve

the electrochemical performance of FIBs.[16–22] Nanocrystalline fluorite-type (cubic, *Fm*-3*m*) solid solutions have also been explored for their interesting fluoride conductivity properties.[23–25] However, the electrochemical stability of solid fluoride electrolytes has never been investigated so far. The investigation of the electrochemical stability window is crucial to determine the potential range in which the cell can operate without degradation of the electrolyte. This is perfectly illustrated by advances in the field of solid-state lithium ion batteries. Despite the efforts made by the community to develop solid electrolytes capable of ionic conductivities equivalent to those of liquids[26], the high-rate capability of cells using such electrolytes remains inferior.[27] These efforts have recently been focused on interfacial phenomena which are the cause of the slow electrochemical kinetics.[28–30] It is now fair to say that the principle obstacle for developing all-solid-state batteries capable of delivering relatively high current densities relies in the achievement of low resistance interfaces.[31] Electrochemical stability of the electrolyte and electrochemical/chemical compatibility with the cell components is therefore crucial to avoid the formation of interphases and layers that can significantly impede mass and/or charge transport. Analogous observations can be made for solid fluoride electrolytes.

In this work, we discuss the fundamental challenges inherent to the use of fluoride-ion conductors in rechargeable batteries. **Figure 1** shows a schematic of a typical solid state fluoride ion battery illustrating the challenges we aim to discuss. To allow for reversible electrochemical reactions, suitable electrochemical stability of the electrolyte must be ensured. Moreover, ionic and electronic conduction must be achieved throughout the composite electrode. The ionic and electronic conduction in this electrode is typically ensured by adding a solid electrolyte and carbon. This practice therefore raises the question of the interaction of fluoride ions with carbon to yield insulating carbon fluorides CF_x, as previously mentioned by Nowroozi *et al.*[13]

Addressing these challenges is significantly complexified by both the lack of reference electrode and lack of inert electrode against fluorination. While electrochemical investigations in metal-ion batteries

are generally performed using the corresponding metal as a reference electrode, no such equivalent exists for FIBs, as the elemental form of fluoride is fluorine gas, F_2. Concerning the study of the electrolyte electrochemical stability window, this is typically done using an electrode which is inert against the electrolyte oxidation. In Li-ion batteries, noble metals like platinum are used as inert electrodes as they are stable at high potentials, where electrolyte decomposition occurs. They are only limited by Li-alloying reactions at potential < 0.2 V *vs.* Li^+/Li.[32] In FIBs, the electrolyte decomposition is accompanied by fluorine evolution, which is highly reactive and able to form compounds with all materials typically used as inert electrode.

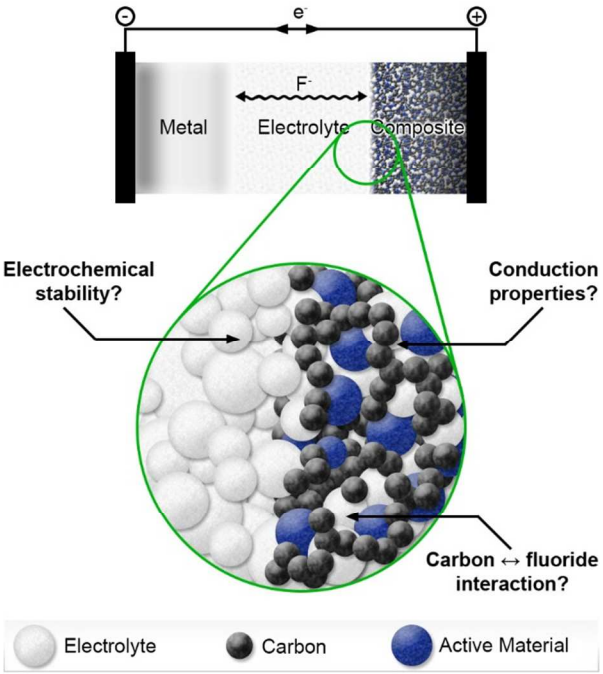

Figure 1. Schematic representation of a solid state fluoride ion battery with a zoom in on the interface between the electrolyte and the composite electrode. The arrows and questions illustrate the challenges that need to be addressed.

In an attempt to meet these challenges, we selected nanocrystalline LBF as model solid electrolyte since it exhibits a relatively high ionic conductivity (about 10^{-4} $S.cm^{-1}$ at 160 °C[20]) and its conduction properties have been extensively studied.[18,20,22] Moreover, LBF was successfully used in FIBs.[2,13,14,33–35]

First, the suitability of Li as electrode for FIBs is assessed by time resolved electrochemical impedance spectroscopy (EIS). Secondly, the electrochemical stability of LBF is studied using Li and Pt electrodes. Thirdly, the electronic and ionic conductivity of a LBF-carbon (LBF-C) composite is investigated and finally, the LBF-C is used to assess the interaction of carbon with fluorides.

Experimental Section

Characterizations. Powder X-ray diffraction (XRD) measurements were performed using a Rigaku Ultima IV diffractometer with a Cu Kα radiation (λ = 1.5418 Å), at a 2θ scan rate of 0.1°/min and a step of 0.017°, between 10° and 80°. Transmission electron microscopy (TEM) images were obtained with a JEOL JEM 2011 on carbon coated copper grids impregnated by a suspension of the material in ethanol.

Preparation of the materials. The electrolyte, $La_{0.95}Ba_{0.05}F_{2.95}$ (LBF), was prepared by ball-milling LaF_3 (Alfa Aesar, 99.99 %) and BaF_2 (Strem chemicals, 99.99 %) in N_2 atmosphere at 400 rpm for 12 hours with a Fritsch pulverisette 7 premium line planetary ball mill with ZrO_2 jars and milling balls (10 mm diameter). The detailed preparation of the electrolyte and the influence of the milling parameters on its purity is detailed in the work of Chable *et al*.[22] The XRD pattern of LBF can be found in **Figure S2** and a presentation of its crystal structure in **Figure S3**. The LBF-C composite was obtained by an additional milling step using the obtained LBF powder (90 wt %) and carbon black (Pure Black, Superior Graphite, 10 wt %, see supporting information for details), denoted C. The mixture was ball-milled in conditions similar as LBF preparation, for 4 hours. The carbon black was first outgassed for 12h at 150 °C. Graphite (Cg) disks were cut from high purity graphite rods (Mersen, ⌀10 mm), polished (P400 SiC abrasive paper), sonicated 3 times in ultrapure water and dried overnight under vacuum at 150 °C. Typical thickness of the graphite disks was 0.5 – 0.7 mm. Lithium foil (99.9%) was purchased from Sigma Aldrich, and Pt foil (99.9 %) was polished (P2400 SiC abrasive paper) and rinsed before

use. Silver (Ag) conductive paint (RS Components) was painted on the LBF surface and dried at 150 °C under vacuum for 12 h.

Cell assembly. Powders were pressed into 10 mm pellets at 5 t in a dry Ar glove box. The Li|LBF|Li and Li|LBF|Pt cells were obtained by placing a pre-compacted LBF pellet (300 mg) between Li or Pt disks. For the Ag|LBF|LBF-C|LBF|Ag cell, 30 mg of LBF-C and 300 mg of LBF powders were stacked and pressed in a single step, and the pellet painted with Ag paint on each side. For the Li|LBF|LBF-C and Li|LBF|C cells, a Cg disk was added to form LBF|LBF-C|Cg and LBF|C|Cg pellet stacks, using 15 mg of LBF-C and 5 mg of C, respectively. The stacks were then laid on a Li disk. All cell preparation and assemblies were carried out in a dry Ar glove box. A summary of the cell configurations used in this study is available **Figure S1** (supporting information). The stacks described above were mounted in modified CR2032 coin-cells. A flat PTFE washer of the desired thickness was used to maintain the stack at the center of the coin cell. A flat spring was used to maintain electrical between the stack and the coin-cell case. Spacers (stainless steel disks) were used to adjust the thickness of the pellet stack to the space available in the coin-cell. The crimped coin-cells were then tightened on a custom made electrochemical test bench employing a screw system, so that the stacks could remain under constant pressure for the duration of the electrochemical measurements. The test bench was placed in an oven set to 30 °C. The cells were left at the designated temperature for at least 3 hours to allow reaching thermal equilibrium before electrochemical measurements.

Electrochemical measurements. Electrochemical impedance spectroscopy (EIS) was recorded in the 13 MHz – 5 Hz frequency range, with a HP 4192A LF impedance analyzer, or in the 300 kHz – 3 mHz frequency range, with a BioLogic VSP potentiostat equipped with a low current extension. The amplitude of the sinusoidal potential excitation was adjusted in the 43 mV – 300 mV range depending on the impedance of the cell, after checking the linearity of the measurement. Impedance spectra were fitted using EC-Lab Zfit. Cyclic voltammetry (CV) was recorded at 30 °C with a BioLogic VSP

potentiostat channel equipped with a low current extension. All experiments were carried out at a scan rate of 0.1 $mV.s^{-1}$ between 7 V and -0.2 V, starting from OCV.

The ohmic drop was corrected using the resistance of the electrolyte determined from EIS measurements. The current density, rather than the current, was used to allow comparison of the cells during the investigation of the electrochemical compatibility of LBF with carbon. The contact area A of the LBF|WE (working electrode) developed at the interface was estimated using the relation:

$$A = \frac{L}{\sigma_i(LBF).R_{gb}}$$

With L the thickness of the LBF layer, σ_i the LBF conductivity at 30°C determined from conductivity measurements on the Ag|LBF|Ag cell, and R_{gb} the resistance of the electrolyte determined from EIS measurements on the relevant cell (see the supporting information for a detailed interpretation of the EIS spectra obtained from the conductivity measurements). The thickness of the electrolyte was measured with a micrometer and assumed to be the same for all experiments as the same mass of LBF was used.

^{19}F solid state Nuclear Magnetic Resonance (NMR). ^{19}F solid-state Magic Angle Spinning (MAS) NMR spectra were recorded on an Avance III Bruker spectrometer operating at 7 T (^{19}F Larmor frequency of 282.2 MHz), using a 1.3 mm diameter probe head allowing spinning frequencies up to 70 kHz. One dimensional (1D) NMR spectra were recorded using a Hahn echo sequence for which interpulse delay was synchronized with the rotor spinning frequency. A 90° pulse length of 1.25 µs was used, recycle delays of 2 s were applied and 128 transients were accumulated. Due to air frictional heating, the sample temperature varied by up to 32°C from 34 to 64 kHz (^{207}Pb isotropic chemical shift of $Pb(NO_3)_2$ was used as a NMR thermometer[36,37]). The maximum temperature gradient over the dimension of the 1.3 mm rotor was estimated to be around 8°C. The ^{19}F chemical shifts are referenced to $CFCl_3$ at 0 ppm.

Results & Discussion

1. Interface of LBF with lithium and electrochemical stability

Lithium metal was selected as counter electrode as it offers practical advantages such as a relatively low oxygen sensitivity (compared to lanthanides[33]) and softness, providing good contact with the solid electrolyte. Due to the low potential of Li, reaction of LBF to yield LiF and metallic La (and Ba) is expected according to:

$$MF_x + x\text{Li} \rightarrow x\text{LiF} + M \quad (1.)$$

The calculated Gibbs free energies ($\Delta_r G° = -120$ kJ.mol^{-1} and -15 kJ.mol^{-1} for LaF_3 and BaF_2, respectively) of the corresponding reactions indicate that spontaneous reduction of LBF must occur. The formation of the interface should provide a convenient pseudo-reference redox couple as long as the interface is not entirely blocking. To investigate the interface properties of Li with LBF, a Li|LBF|Li cell was assembled and monitored by time-resolved electrochemical impedance spectroscopy (EIS) (**Figure 2**).

After 3 hours of contact, the impedance spectrum exhibits a complete semi-circle and an additional semi-circle, followed by a capacitive tail. The first semi-circle is characteristic of the electrolyte's ionic resistance and is denoted R_{gb} (see supporting information for more details). Over time, the resistance of the first semi-circle is stable, while the resistance of the second semi-circle increases. The fitting of all spectra was carried out with the equivalent circuit presented on **Figure 2 (c)**. The resistances of the two semi-circles, gathered from the fits, are reported on **Figure 2 (b)**.

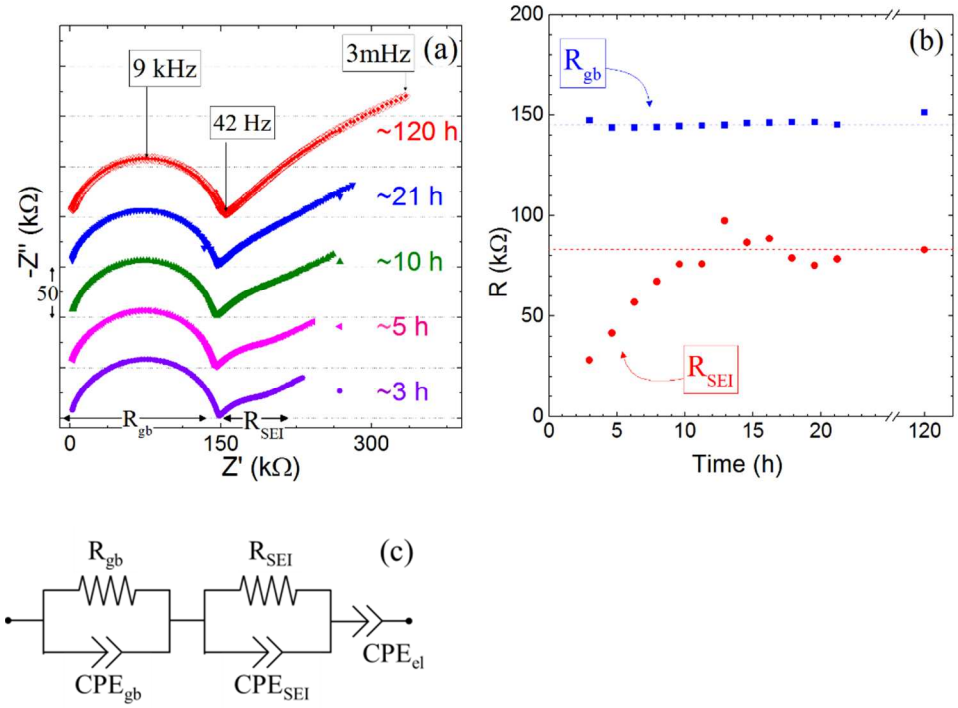

Figure 2. (a) Nyquist plot of the impedance spectra of a Li|LBF|Li cell in open circuit conditions at 30 °C. The frequency, in Hz, of a few points is indicated for comparison with **Figure S4** (b) Evolution of Rgb and Rlayer in function of time under open circuit conditions. (c) Equivalent circuit used to fit the data.

The appearance of a second semi-circle is attributed to the expected formation of a LiF|La-Ba interface layer resulting from the localized oxidation of Li to LiF and reduction of LBF to a La-Ba mixture. This layer can be described as a solid electrolyte interface (SEI) and its resistance is therefore denoted R_{SEI}. While the value of R_{gb} does not significantly vary over time, R_{SEI} gradually increases and stabilizes at around 82 kΩ after 15 h. Accordingly, the increase of R_{SEI} prior to its stabilization can be ascribed to the increase of the thickness of the SEI until it becomes sufficiently thick to impede significant local charge/mass transfer, and reach equilibrium. Nonetheless, R_{SEI} (≈ 41 kΩ for a single Li|LBF interface) is inferior to the electrolyte resistance R_{gb} (≈ 145 kΩ) so that the overall cell impedance remains sufficiently low to perform electrochemical characterizations. All these observations suggest that Li is a suitable electrode for the measurement of the electrochemical stability of fluoride solid electrolytes.

To evaluate the experimental electrochemical stability of LBF, a Li|LBF|Pt cell was assembled and cyclic voltammetry was performed at 0.1 mV/s scan rate, at 30 °C (**Figure 3**). The cell was polarized up to 7 V and down to -0.5 V, for two cycles. Two main features can be observed. One is the occurrence of redox peaks at around 0 V. The other is the oxidation current observed beyond 5 V. The redox peaks at around 0 V are typically observed with Li^+ conducting electrolytes in analogous cells (Li|Li-electrolyte|Pt) and are generally attributed to the lithium plating/alloying and stripping (reduction and oxidation) at the Pt electrode and concomitant lithium oxidation and reduction at the Li electrode[26,38–41]. Considering the structure of LBF, it is unlikely that Li^+ can migrate through the electrolyte from the Li electrode to the Pt electrode. Therefore, the redox peaks around 0 V can be assigned to redox reactions involving LBF at both the Li and Pt electrode (*i.e.*, $La/Ba_{(s)} + 3F^- \leftrightarrow LBF_{(s)} + 3e^-$). These observations suggest that the SEI exhibits some reversibility, although further characterization would be needed to confirm this observation.

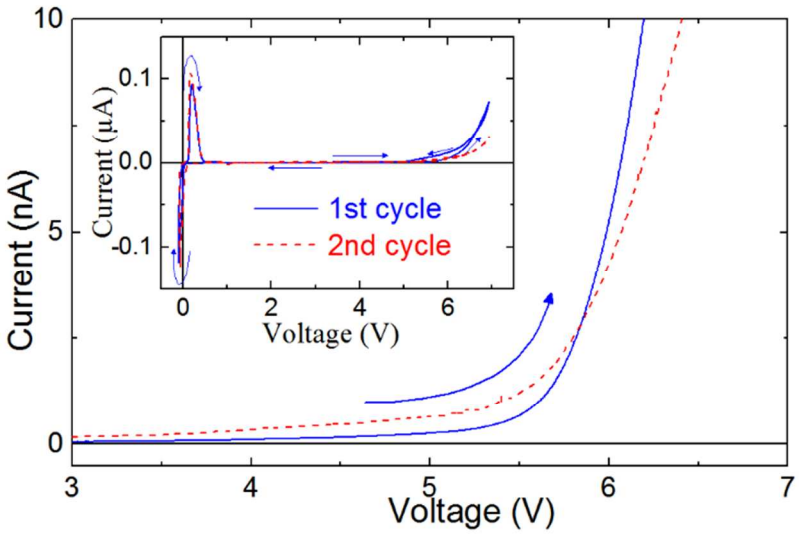

Figure 3. Cyclic voltammograms (forward scans from 3 to 7 V) of the Li|LBF|Pt cell performed at a 0.1 mV/s scan rate, at 30 °C. Inset: full scans between -0.05 and 7 V.

The steep increase of the oxidation current beyond 5 V can be ascribed to the electrochemical decomposition of LBF. The decomposition potential can be calculated from thermodynamic data by considering the following reaction:

$$MF_{x\,(s)} \rightarrow M_{(s)} + \frac{x}{2} F_{2\,(g)} \qquad 2.$$

The theoretical potential of such reaction is given by the following equations:

$$\Delta_r G° = -nF\Delta E° = \Delta_f H° - T\Delta S° \qquad 3.$$

with n the number of moles of electrons exchanged upon decomposition, F the Faraday constant (96485 C.mol^{-1}), T the absolute temperature (K), and $\Delta_f H°$ (kJ.mol^{-1}) and $\Delta S°$ (kJ.mol^{-1}.K^{-1}) are respectively the standard enthalpy and entropy of the reaction. Calculations based on the aforementioned equations using thermodynamic data from The Materials Project[42] yield ΔE° of 5.73 V and 6.00 V for LaF_3 and BaF_2, respectively, which is in good agreement with the value of 5.811 V calculated by Roos and Schoonman for LaF_3.[43] The calculated decomposition potential of LaF_3 is in good agreement with our experimental observations as the current dramatically increases beyond 5.8 V. Although, it is obvious that the current significantly increases before the calculated thermodynamic value of 5.73 V. This current may be attributed to the fluorination of the Pt electrode prior to F_2 evolution. The fluorination of Pt is further suggested by the less steep increase of the decomposition current in the 2nd cycle (dashed line on **Figure 3**) which could be explained by the insulating effect of the PtF_x layer formed on the surface of Pt electrode during the 1st cycle. For instance, the calculated potential of the reaction of Pt with LaF_3 (e.g. 3 Pt + 2 LaF_3 → 3 PtF_2 + 2 La) is ~4.17 V based on thermodynamic data of PtF_2 from Glassner[44]. Therefore, polarization of a Li|LBF|Pt cell beyond 4.17 V induces LBF reduction at the Li electrode, and F_2 evolution and/or Pt fluorination at the Pt electrode. Experimental observations made by Bezmelnitsyn et al.[45] are in agreement with this mechanism. They polarized a M|LBF|M cell (M = Ni, Cu or graphite) by applying a galvanostatic current of 1.0 mA and observed F_2 evolution and the formation of La/Ba dendrites at the negative electrode. XPS analysis of the dendrites showed that it was

a mixture of La and Ba metal with a Ba/La ratio corresponding to that in the LBF. Our experimental observations are summarized by the schematic illustration of the decomposition mechanism displayed on **Figure 4**.

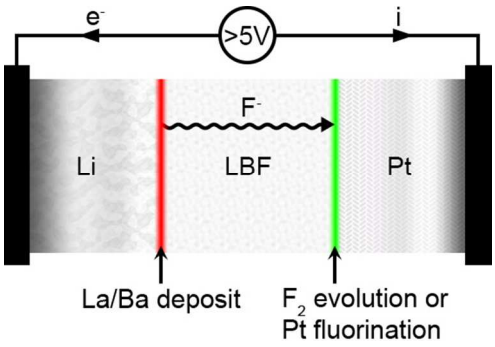

Figure 4. Schematic illustration of the decomposition mechanism of LBF.

In conclusion, we established that lithium is a suitable electrode for the measurement of the electrochemical stability of solid fluoride electrolytes. The SEI formed upon contacting Li with the fluoride solid electrolyte is not entirely blocking, and the presence of the LiF|La-Ba interface layer provides a redox couple that can be conveniently used to evaluate the electrochemical stability of the solid fluoride electrolyte. It must be noted that since the LiF would form in contact with the Li surface and the La-Ba mixture in contact with the LBF, the interface can be noted as Li|LiF|La-Ba|LBF. It can therefore be expected that the redox couple created at the Li|LiF|La-Ba|LBF interface is the LBF/La-Ba couple (i.e., La^{3+}/La and Ba^{2+}/Ba), the LiF|Li interphase acting as "current collector". This result is promising as it is the first step in addressing a major challenge inherent to the study of FIBs, which is the lack of a reference electrode. Further work is required to verify whether this interphase provides a proper reference electrode, *i.e.*, the LBF/La-Ba couple at the interface is kinetically fast enough to provide a non-polarizable electrode. Nonetheless, the LBF/La-Ba couple provides a baseline from which thermodynamic calculations of the cell redox potentials can be performed. The potentials obtained from those calculations can be used to assign variations of the cell measured current to possible electrochemical reactions, bearing in mind the possible presence of overpotentials.

As for the electrochemical stability of LBF, we can conclude that its theoretical decomposition potential (5.73 V), corresponding to F_2 evolution at the Pt electrode, is largely above the theoretical potential at which the working electrode would be fluorinated. In our Li|LBF|Pt cell, we observed the apparition of an oxidation current at potentials below that of the theoretical decomposition potential of LBF. This can be explained by the fluorination of Pt prior to F_2 evolution at the Pt electrode or by the catalytic effect of the Pt. Experimental observations of the actual decomposition potential will be very challenging considering that unlike in metal-ion batteries, there is effectively no inert material against fluorine-ion. Therefore, we propose that the best way to avoid reduction of the electrolyte is to calculate the redox potential of electrochemical reactions involving both the FIBs' active materials and the electrolyte to verify that the redox potential of reactions involving the active materials are below the redox potential of reactions involving the electrolyte. In the case of solid solutions like LBF, we suggest doing thermodynamic calculations using the electrolyte components (LaF_3 and BaF_2) as no thermodynamic data are available for LBF. For instance, in a Bi|LBF|MgF_2 cell, the calculated redox potential of the reaction 2 Bi + 3 MgF_2 ↔ 2 BiF_3 + 3 Mg is 2.65 V, below the values calculated for reactions involving LaF_3 and BaF_2, i.e., Bi + LaF_3 ↔ BiF_3 + La (2.83 V) and 2 Bi + 3 BaF_2 ↔ 2 BiF_3 + 3 Ba (3.11 V). Reduction of MgF_2 should therefore occur before reduction of LBF.

2. Structural and electrical characterization of the LBF-C composite.

Metal fluorides are generally poor electronic conductors due to their large band gap, as predicted by the band theory (e.g 4.681 eV for BiF_3[42]). Their use as active material requires the development of composites containing electronic conductive additives to ensure the electronic percolation in the electrode. This is typically achieved by mixing carbon black, or other carbonaceous materials, with the active material. Ball-milling is a common method to produce metal fluoride-carbon nanocomposites that

present good performance in conventional lithium-ion batteries.[46] The same approach can be used to produce electrode composites for solid-state lithium and fluoride-ion batteries.

Additionally, solid electrolyte must be mixed with the active material and the carbonaceous additive to achieve ionic conductivity within the electrode. Despite the fact that some metal fluorides available as active material offer ionic conductivity properties (e.g. $\sigma_i \approx 1\times10^{-6}$ S.cm^{-1} at RT for cubic BiF_3[10]), their ionic conductivity is generally lower than that of LBF. Besides, upon operation of the FIB, the metal fluoride will lose its ionic conductivity properties when reduced to its metallic state. Therefore, both carbon and electrolyte must be present in the electrode composites to ensure electronic and ionic conductivity through the bulk of the electrode. This raises the question of the interaction of carbonaceous additives with the fluoride conducting electrolyte, both upon preparation of the electrode materials and upon operation of the cell. Indeed, the fluorination of the carbonaceous material to yield insulating graphite fluorite, CF_x, would be detrimental to the electrochemical performance of the electrode.

To address this question, LBF and carbon black were mixed in a 9:1 weight ratio and ball-milled to yield the LBF-C composite. The influence of ball-milling on the structure and composition of the starting materials was investigated, the electrical properties of the LBF-C composite were measured by means of electrochemical impedance spectroscopy, and the LBF-C was used as working electrode in a Li|LBF|LBF-C to assess the fluorination of carbon.

a. Structural characterization of the LBF-C composite.

The XRD pattern of the LBF-C composite (**Figure S5**) indicates that no observable structural modification of LBF takes place during the ball-milling process. The possible formation of CF_x during ball-milling ($LaF_3 + C \rightarrow LaF_{3-x} + CF_x$)[47] was investigated using ^{19}F NMR (**Figure S6**). ^{19}F NMR shows no sign of the formation of CF_x groups typically characterized by resonances in the -50 – -300 ppm region.[48–50] NMR further confirms that no changes occur in LBF as the ^{19}F signal gives identical shifts

before and after ball milling. TEM images (**Figure S7**) show agglomerates of LBF of size ranging from a few dozen to several hundred nanometres, surrounded by large agglomerates of carbon black particles.

b. Electrical characterization of the LBF-C composite.

The electrochemical properties of the LBF-C composite was first investigated by EIS performed on a graphite|LBF-C|graphite cell denoted Cg|LBF-C|Cg thereafter. A Cg|Cg cell was used as a blank to deduct the electronic conductivity of the composite. Figure 5 shows the impedance spectra of the Cg|LBF-C|Cg and Cg|Cg cells recorded at 30 °C. The presented impedance spectra are characteristic of electronic conductors (single resistor), but present an inductive contribution at high frequencies, due to the wiring of the measurement setup. The Nyquist plot of a resistor ($Z_R = R$) is characterized by a single value on the x axis, yielding its resistance.

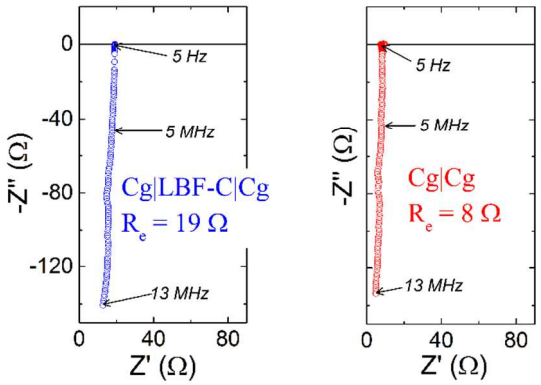

Figure 5. Impedance spectra of a Cg|LBF-C|Cg (a) and Cg|Cg (b) cell at 30 °C (Cg = carbon graphite disk).

The intersection of the inductive tail with the x axis (-Z'' = 0) gives the electronic resistance of the cell, R_e, yielding values of 19 Ω and 8 Ω, for Cg|LBF-C|Cg and Cg|Cg, respectively. An electronic resistance of 11 Ω is deduced for the LBF-C composite, yielding an electronic conductivity, σ_e, of about 10^{-2} $S.cm^{-1}$. This result suggests that the electronic percolation threshold is reached for 10 wt % C. Moreover, the electronic conductivity of LBF-C is several orders of magnitude higher than the ionic conductivity of

pure LBF (almost 5 orders of magnitude at 30 °C), indicating that the electronic conductivity of the composite electrode is not the rate limiting phenomena.

The determination of the ionic conductivity of the LBF-C composite in the Cg|LBF-C|Cg setup is not possible due to shorting created by the carbon present in the composite, as illustrated on **Figure 6**. To counter this, LBF can be used as an electronically blocking electrode. The electrons are blocked at the LBF|LBF-C interface so that the electronic conductivity of LBF-C does not short circuit the cell. Consequently, the ionic conductivity of both LBF and LBF-C can be determined.

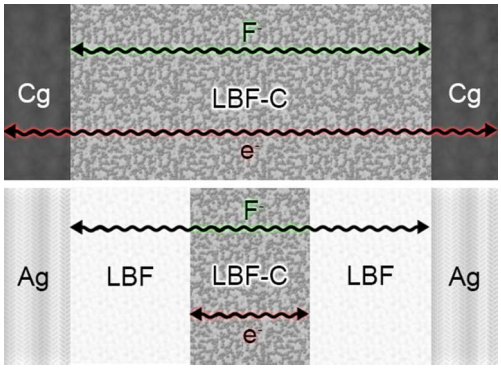

Figure 6. Schematic representation of the Cg|LBF-C|Cg and Ag|LBF|LBF-C|LBF|Ag cells used to determine the electronic and ionic conductivity of LBF-C, respectively. Schematic electronic (e-) and ionic (F-) migration routes are shown for the sake of clarity.

The impedance spectrum of the Ag|LBF|LBF-C|LBF|Ag cell recorded at 30 °C is shown on **Figure 7**. The spectrum of a Ag|LBF|Ag cell recorded at the same temperature is also added for comparison. Both spectra present a semi-circle, characteristic of the ionic conductivity, followed by a capacitive tail, characteristic of blocking effects at the Ag electrodes. The frequency shift observed for the stack configuration when compared to the sole LBF might be due to the slower migration of F^- in the LBF-C layer, thus increasing the characteristic time of the process, thus decreasing the characteristic frequency.

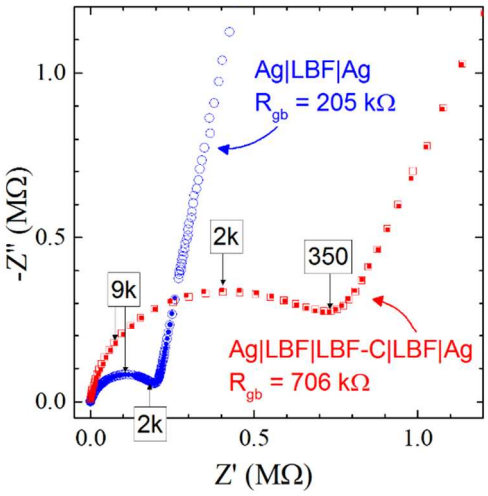

Figure 7. Nyquist plot of the impedance spectra of the □ Ag|LBF|LBF-C|LBF|Ag and ○ Ag|LBF|Ag cells recorded at 30 °C. The open symbols represent the data and the closed symbols represent the fits obtained.

The ionic conductivity of the LBF-C layer can be determined by subtracting the contribution of the LBF layers. The resistance of the LBF-C layer corresponds to the resistance of the Ag|LBF|LBF-C|LBF|Ag stack (706 kΩ) minus the resistance of the two LBF layers (2×205 kΩ). A resistance of 296 kΩ is obtained for the LBF-C layer yielding an ionic conductivity of 5×10^{-8} S.cm^{-1} at 30 °C. This value is about one order of magnitude lower than the ionic conductivity of LBF alone (5.4×10^{-7} S.cm^{-1}, see supporting information) showing that the ionic percolation is maintained but also affected by the preparation of the LBF-C composite.

The fluoride ions mobility in the LBF-C composite was further investigated by ^{19}F MAS NMR (Figure **8**). As previously reported for LBF, the F2 and F3 NMR resonances (having the largest isotropic chemical shifts) are no longer resolved and partially overlap with that of F1 (preventing reliable calculations of their relative intensities)[18]. These broadenings reflect the enhanced disorder induced by the ball milling technique. In the tysonite type solid solutions $La_{1-x}M_xF_{3-x}$, because F1–F1 exchanges are considerably faster than F1–F2,3 exchanges, the exchange between F1 and F2,3 results in a shift toward a larger frequency of the NMR resonance assigned to F1 and in a decrease of the relative intensity of the

F2,3 resonances.[17,18] This is what is observed, when the temperature increases, for the LBF-C composite, to a similar extent as LBF,[18] showing that the fluoride ions mobility is not impacted by the presence of carbon.

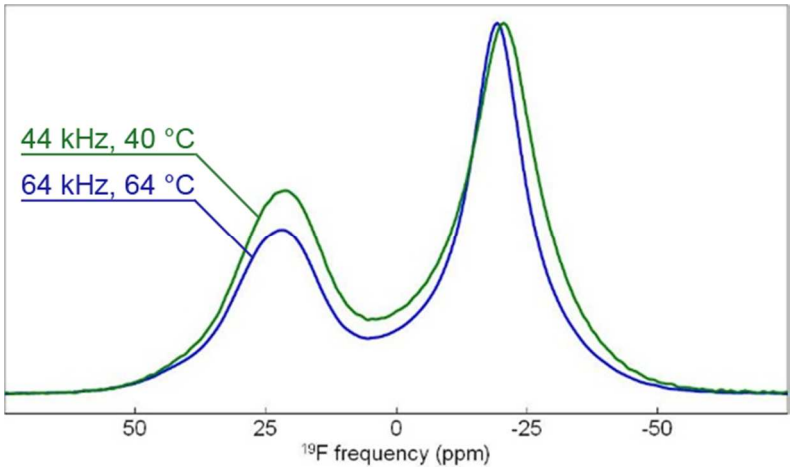

Figure 8. ^{19}F MAS (64 kHz at 64°C, and 44 kHz at 40°C) NMR spectra of LBF-C.

Note that, the precise way the carbon interacts with LBF, *i.e.*, only due to morphology effects, or together with grain boundary effects, could be investigated in more details using dielectric spectroscopy[51].

In summary, the investigation of the electrical properties of the LBF-C material revealed that both electronic ($\sigma_e \approx 10^{-2}$ S.cm^{-1}) and ionic percolations ($\sigma_i \approx 5\times10^{-8}$ S.cm^{-1}) are insured within the composite. The methodology adopted here provides a versatile tool to optimize the composite electrode by obtaining the best compromise between electronic and ionic conductivity.

3. Electrochemical activity of carbon

While in lithium batteries, it is well established that carbonaceous additives may contribute to the overall capacity due to the insertion of lithium ions at low potential, the possible electrochemical fluorination of carbon in FIBs is still an open question[13]. It is particularly important to address this question since the fluorination of carbon yields CF_x compounds which are electronic insulators. To investigate potential reactions with carbon, the electrochemical reactions occurring in Li|LBF|C and

Li|LBF|LBF-C cells were compared with a benchmark cell with no carbon, *i.e.*, Li|LBF|Pt cell. The cells were polarized up to 7 V. The complete CV scans on Li|LBF|C and Li|LBF|LBF-C cells can be found in supporting information (**Figures S7** and **S8**, respectively). **Figure 9** shows the first cycle forward scans from 3 V up to 7 V and their corresponding derived curves for Li|LBF|Pt (from **Figure 3)**, Li|LBF|C and Li|LBF|LBF-C cells.

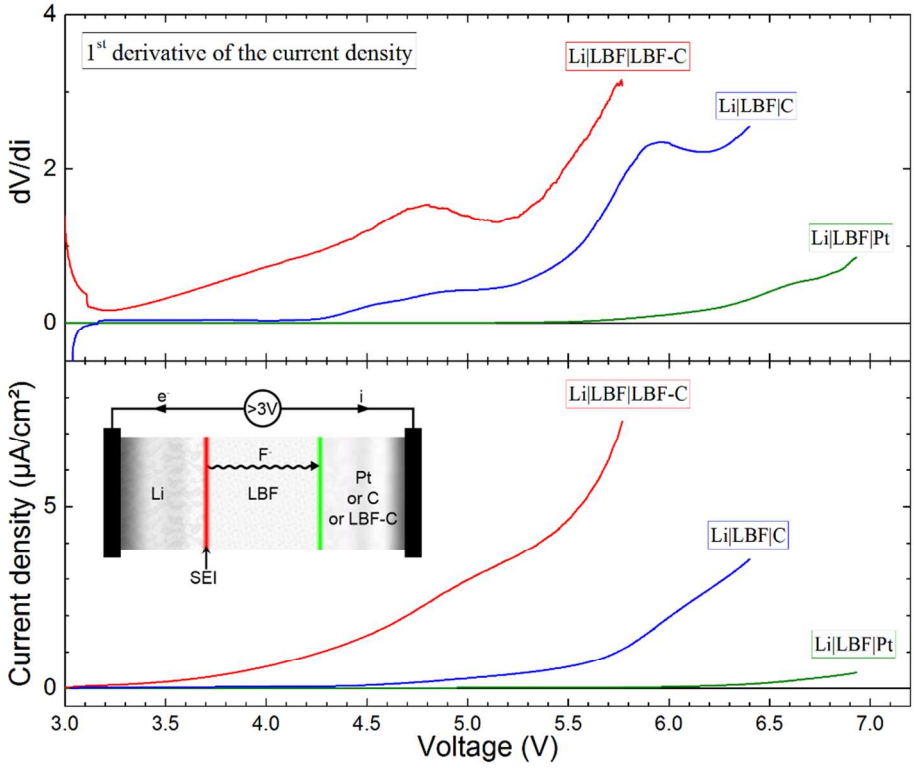

Figure 9. Overlaid forward CV scans and their 1st derivatives for the 3 Li based cells with different working electrodes: Pt, C and LBF-C. The curves were corrected for iR drop and normalized with the current density. Inset: schematic representation of the polarized cell illustrating the migration of fluoride ions towards the working electrode.

Upon polarization, fluoride ions are moving from the cathode side (SEI) towards the Pt or carbon-based working electrode anode, as represented on the schematic in inset of **Figure 9**. To ease the

discussion, the cells will be referred by the name of their respective electrode (*i.e.*, Pt cell, C cell and LBF-C cell).

The voltammogram of the benchmark cell (Pt) was previously discussed (**Figure 3**) and is added for comparison. The earlier onset of the current can be attributed to fluorination of Pt before F_2 evolution.

In the presence of carbon, *i.e.*, LBF-C and C cells, the current increases at lower voltages. The derivative curves feature two main contributions located at 4.2-4.8 V, and beyond 5.2 V. The later can be assigned to the electrochemical decomposition of the electrolyte. The early onset of the decomposition of LBF in the LBF-C cell might be due to the increased contact area between the solid electrolyte and the carbon that accelerates the kinetic of the reaction.[52] The increase of the current at lower voltages (4.2-4.8 V) suggests an electrochemical reaction of carbon. Carbon might react with LaF_3 (and/or BaF_2) from LBF to yield CF_x as follow:

$$\frac{1}{3}LaF_3 + C \rightarrow CF + \frac{1}{3}La \qquad 4.$$

The standard potential of the electrochemical fluorination reaction of carbon was calculated using the enthalpy of formation of CF_x obtained from the literature. According to Valerga *et al.*[53], the entropy and enthalpy of formation of CF_x depends on the F/C ratio and can be calculated (at 298 K) as follows:

$$\Delta_f H^0_{CF_x} = (4.53 - 178.01\,x)\ kJ.mol^{-1} \qquad 5.$$

$$S^0_{CF_x} = (4.62 - 16.91\,x)\ J.K^{-1}.mol^{-1} \qquad 6.$$

The calculated potential for the formation of CF is about 4.19 V for a reaction involving LaF_3 and 4.47 V for a reaction involving BaF_2. The value of 4.19 V is close to the first contribution to the current observed on the CV of the C and LBF-C cells, suggesting that carbon undergoes electrochemical fluorination to form CF_x. This is particularly clear for the C electrode, as the

derivative shows a significant increase of the current observed at about 4.3 V, which is concomitant with the calculated potential for the reaction of LaF_3 to form CF_x at the LBF|C interface (4.19 V). The slight change of slope at about 4.5 V might be due to the onset of reactions involving the Ba^{2+} of LBF to form CF (4.47 V). Finally, a frank change of slope is observed above 5.5 V, which corresponds to the decomposition of LaF_3 from LBF (5.73 V) to yield elemental fluorine. In the case of the LBF-C cell, it is difficult to accurately determine the onset of the current related to the carbon reactivity as current increases as soon as the cell is polarized. This phenomenon may be attributed to non-faradaic (i.e. capacitive) processes building up at the interface between LBF and C. Nonetheless, the CV derivative of the LBF-C cell yields a similar shape than that of the C cell so that similar conclusions can be made about the fluorination of carbon.

Our observations about the carbon's electrochemical activity with fluoride is in good agreement with the work of Nowroozi *et al.*[13] who showed that the electrochemical fluoride ion insertion into $LaSrMnO_4$ is accompanied by an extra capacity that can be attributed to the fluorination of carbon to form CF_x. Because CF_x compounds exhibit insulator properties due to the covalent nature of the C-F bond inducing a sp^3 hybridization in these compounds[54], the progressive fluorination of the carbon might eventually lead to a progressive loss of the operational electronic conduction pathways. One might consider that the electrochemical window needs to be narrowed to avoid the formation of carbon fluorides, as these processes are generally considered to be irreversible.

Another possible interaction of carbon with fluorides might be the formation of graphite intercalation compounds (GICs) in which intercalation might be reversible, as it is the case in lithium-ion batteries. To the best of our knowledge, no thermodynamic data are available on these compounds so that no theoretical voltage could be calculated. Further experiments must be carried out to explore this possibility.

Conclusion

The electrochemical stability and electrical properties of nanocrystalline fluoride solid electrolyte $La_{0.95}Ba_{0.05}F_{2.95}$, LBF, have been investigated both in its pure form and in a composite with carbon. Electrochemical characterizations have been performed using a lithium electrode. Upon contacting Li with the solid fluoride electrolyte, a solid electrolyte interface (SEI) of LiF and La-Ba mixture is formed, providing the LBF/La-Ba redox couple. This method has allowed us to establish the decomposition potential of LBF beyond 5.7 V, in good agreement with the calculated value. Subsequently, the electrical properties of the composite LBF-carbon was investigated using a conventional set up. It showed that only the electronic conductivity could be assessed, revealing that 10 wt % of carbon is sufficient to enable electronic percolation. The determination of the ionic conductivity within the composite was probed by a novel set up consisting of LBF|LBF-C|LBF stacks. The results showed that the ionic percolation is maintained within the LBF-C composite and that the interactions with carbon impacts on the ionic transport properties of the electrolyte. Finally, we demonstrated that carbon was electrochemically active in the LBF-C composite. The operating voltage of FIBs must be carefully considered as the fluorination of carbon to yield insulative carbon fluoride could be a serious limitation to the operation of FIBs.

Author Information

Corresponding Author

* E-mail: damien.dambournet@upmc.fr

Abbreviations

FIB, fluoride ion battery; SEI, solid electrolyte interface; EIS, electrochemical impedance spectroscopy; LBF, $La_{1-x}Ba_xF_{3-x}$; C, carbon black; LBF-C, $La_{1-x}Ba_xF_{3-x}$-carbon black mixture; Cg, graphite disk, CF_x, carbon fluoride compounds.

Supporting Information

XRD pattern and ^{19}F NMR of LBF and LBF-C, TEM images of LBF-C, representation of tysonite-type structure, ionic conductivity of LBFand complete cyclic voltammetry (-0.1 to 7V) of Li|LBF|C and Li|LBF|LBF-C cells are given in supporting information.

Acknowledgement

We gratefully acknowledge J. Chable and A. Gil-Martin for the preparation of the solid fluoride electrolyte, S. Casale for the TEM images, D. Devilliers for fruitful discussions about electrochemical measurements, and S. Leclerc for technical support. AG, HG and DD wish to thank the French Fluorine network for their continuous support.

Funding Sources

This work was funded by the French National Research Agency (Project FLUOBAT-ANR-12-PRGE-0009-01).

References

(1) Gschwind, F.; Rodriguez-Garcia, G.; Sandbeck, D. J. S.; Gross, A.; Weil, M.; Fichtner,

M.; Hörmann, N. Fluoride Ion Batteries: Theoretical Performance, Safety, Toxicity, and a Combinatorial Screening of New Electrodes. *J. Fluor. Chem.* **2016**, *182*, 76–90.

(2) Anji Reddy, M.; Fichtner, M. Batteries Based on Fluoride Shuttle. *J. Mater. Chem* **2011**, *21*, 17059–17062.

(3) Baukal, W. Electrochemical Secondary Cells Which Contains Only Solid Materials. Patent CA 953780 A1, 1974.

(4) Lucat, C. Etude Des Propriétés de Conductivité Ionique de Quelques Fluorures de Structure Fluorine, Ph.D. Dissertation, Université de Bordeaux I, 1976.

(5) Kennedy, J. H.; Miles, R. C. Ionic Conductivity of Doped Beta-Lead Fluoride. *J. Electrochem. Soc.* **1976**, *123*, 47–57.

(6) Kennedy, J. H.; Hunter, J. C. Thin-Film Galvanic Cell $Pb/PbF_2/PbF_2,CuF_2/Cu$. *J. Electrochem. Soc.* **1976**, *123*, 10–14.

(7) Borger, W.; Hullmeine, U.; Voss, E. Galvanic Cell with Solid Fluoride Ion-Conductive Electrolyte. Patent US 3973990 A1, 1976.

(8) Schoonman, J. A Solid-State Galvanic Cell with Fluoride-Conducting Electrolytes. *J. Electrochem. Soc.* **1976**, *123*, 1772–1775.

(9) Danto, Y.; Poujade, G.; Pistre, J. D.; Lucat, C.; Salardenne, J. A $Pb|PbF_2|BiF_3|Bi$ Thin Solid Film Reversible Galvanic Cell. *Thin Solid Films* **1978**, *55*, 347–354.

(10) Schoonman, J.; Wapenaar, K. E. D.; Oversluizen, G.; Dirksen, G. J. Fluoride-Conducting Solid Electrolytes in Galvanic Cells. *J. Electrochem. Soc.* **1979**, *126*, 709–713.

(11) Schoonman, J.; Wolfert, A. Alloy-Anodes in Fluoride Solid-State Batteries. *J. Electrochem. Soc.* **1981**, *128*, 1522–1523.

(12) Schoonman, J.; Wolfert, A. Solid-State Galvanic Cells with Fast Fluoride Conducting Electrolytes. *Solid State Ionics* **1981**, *3–4*, 373–379.

(13) Nowroozi, M. A.; Wissel, K.; Rohrer, J.; Munnangi, A. R.; Clemens, O. $LaSrMnO_4$: Reversible Electrochemical Intercalation of Fluoride Ions in the Context of Fluoride Ion Batteries. *Chem. Mater.* **2017**, *29*, 3441–3453.

(14) Thieu, D. T.; Fawey, M. H.; Bhatia, H.; Diemant, T.; Chakravadhanula, V. S. K.; Behm, R. J.; Kübel, C.; Fichtner, M. CuF_2 as Reversible Cathode for Fluoride Ion Batteries. *Adv. Funct. Mater.* **2017**, *27*, 1701051.

(15) Grenier, A.; Porras-Gutierrez, A.-G.; Groult, H.; Beyer, K. A.; Borkiewicz, O. J.; Chapman, K. W.; Dambournet, D. Electrochemical Reactions in Fluoride-Ion Batteries: Mechanistic Insights from Pair Distribution Function Analysis. *J. Mater. Chem. A* **2017**, *5*, 15700–15705.

(16) Bhatia, H.; Thieu, D. T.; Pohl, A. H.; Chakravadhanula, V. S. K.; Fawey, M. H.; Kübel, C.; Fichtner, M. Conductivity Optimization of Tysonite-Type $La_{1-x}Ba_xF_{3-x}$ Solid Electrolytes for Advanced Fluoride Ion Battery. *ACS Appl. Mater. Interfaces* **2017**, *9*, 23707–23715.

(17) Dieudonné, B.; Chable, J.; Mauvy, F.; Fourcade, S.; Durand, E.; Lebraud, E.; Leblanc, M.; Legein, C.; Body, M.; Maisonneuve, V.; et al. Exploring the $Sm_{1-x}Ca_xF_{3-x}$ Tysonite Solid Solution as a Solid-State Electrolyte: Relationships between Structural Features and F –

Ionic Conductivity. *J. Phys. Chem. C* **2015**, *119*, 25170–25179.

(18) Chable, J.; Dieudonné, B.; Body, M.; Legein, C.; Crosnier-Lopez, M.-P.; Galven, C.; Mauvy, F.; Durand, E.; Fourcade, S.; Sheptyakov, D.; et al. Fluoride Solid Electrolytes: Investigation of the Tysonite-Type Solid Solutions $La_{1-x}Ba_xF_{3-x}$ (X < 0.15). *Dalt. Trans.* **2015**, *44*, 19625–19635.

(19) Zhang, L.; Anji Reddy, M.; Fichtner, M. Development of Tysonite-Type Fluoride Conducting Thin Film Electrolytes for Fluoride Ion Batteries. *Solid State Ionics* **2015**, *272*, 39–44.

(20) Rongeat, C.; Anji Reddy, M.; Witter, R.; Fichtner, M. Solid Electrolytes for Fluoride Ion Batteries: Ionic Conductivity in Polycrystalline Tysonite-Type Fluorides. *ACS Appl. Mater. Interfaces* **2014**, *6*, 2103–2110.

(21) Dieudonné, B.; Chable, J.; Body, M.; Legein, C.; Durand, E.; Mauvy, F.; Fourcade, S.; Leblanc, M.; Maisonneuve, V.; Demourgues, A. The Key Role of the Composition and Structural Features in Fluoride Ion Conductivity in Tysonite $Ce_{1-x}Sr_xF_{3-x}$ Solid Solutions. *Dalt. Trans.* **2017**, *46*, 3761–3769.

(22) Chable, J.; Martin, A. G.; Bourdin, A.; Body, M.; Legein, C.; Jouanneaux, A.; Crosnier-Lopez, M.-P.; Galven, C.; Dieudonné, B.; Leblanc, M.; et al. Fluoride Solid Electrolytes: From Microcrystalline to Nanostructured Tysonite-Type $La_{0.95}Ba_{0.05}F_{2.95}$. *J. Alloys Compd.* **2017**, *692*, 980–988.

(23) Rongeat, C.; Reddy, M. A.; Witter, R.; Fichtner, M. Nanostructured Fluorite-Type Fluorides As Electrolytes for Fluoride Ion Batteries. *J. Phys. Chem. C* **2013**, *117*, 4943–

4950.

(24) Krahl, T.; Scholz, G.; Kemnitz, E. Solid Solutions CaF_2–YF_3 with Fluorite Structure Prepared on the Sol–Gel Route: Investigation by Multinuclear MAS NMR Spectroscopy. *J. Phys. Chem. C* **2014**, *118*, 21066–21074.

(25) Düvel, A.; Bednarcik, J.; Šepelák, V.; Heitjans, P. Mechanosynthesis of the Fast Fluoride Ion Conductor $Ba_{1-x}La_xF_{2+x}$: From the Fluorite to the Tysonite Structure. *J. Phys. Chem. C* **2014**, *118*, 7117–7129.

(26) Kamaya, N.; Homma, K.; Yamakawa, Y.; Hirayama, M.; Kanno, R.; Yonemura, M.; Kamiyama, T.; Kato, Y.; Hama, S.; Kawamoto, K.; et al. A Lithium Superionic Conductor. *Nat. Mater.* **2011**, *10*, 682–686.

(27) Ohta, N.; Takada, K.; Zhang, L.; Ma, R.; Osada, M.; Sasaki, T. Enhancement of the High-Rate Capability of Solid-State Lithium Batteries by Nanoscale Interfacial Modification. *Adv. Mater.* **2006**, *18*, 2226–2229.

(28) Zhu, Y.; He, X.; Mo, Y. Origin of Outstanding Stability in the Lithium Solid Electrolyte Materials: Insights from Thermodynamic Analyses Based on First-Principles Calculations. *ACS Appl. Mater. Interfaces* **2015**, *7*, 23685–23693.

(29) Richards, W. D.; Miara, L. J.; Wang, Y.; Kim, J. C.; Ceder, G. Interface Stability in Solid-State Batteries. *Chem. Mater.* **2016**, *28*, 266–273.

(30) Cheng, X.-B.; Zhang, R.; Zhao, C.-Z.; Wei, F.; Zhang, J.-G.; Zhang, Q. A Review of Solid Electrolyte Interphases on Lithium Metal Anode. *Adv. Sci.* **2016**, *3*, 1500213.

(31) Luntz, A. C.; Voss, J.; Reuter, K. Interfacial Challenges in Solid-State Li Ion Batteries. *J. Phys. Chem. Lett.* **2015**, *6*, 4599–4604.

(32) Aurbach, D. *Nonaqueous Electrochemistry*; Marcel Dekker Inc: New York, 1999.

(33) Rongeat, C.; Anji Reddy, M.; Diemant, T.; Behm, R. J.; Fichtner, M. Development of New Anode Composite Materials for Fluoride Ion Batteries. *J. Mater. Chem. A* **2014**, *2*, 20861–20872.

(34) Hammad Fawey, M.; Chakravadhanula, V. S. K.; Reddy, M. A.; Rongeat, C.; Scherer, T.; Hahn, H.; Fichtner, M.; Kübel, C. In Situ TEM Studies of Micron-Sized All-Solid-State Fluoride Ion Batteries: Preparation, Prospects, and Challenges. *Microsc. Res. Tech.* **2016**, *79*, 615–624.

(35) Grenier, A.; Porras-Gutierrez, A. G.; Groult, H.; Dambournet, D. Modified Coin Cells to Evaluate the Electrochemical Properties of Solid-State Fluoride-Ion Batteries at 150°C. *J. Fluor. Chem.* **2016**, *191*, 23–28.

(36) Bielecki, A.; Burum, D. P. Temperature Dependence of ^{207}Pb MAS Spectra of Solid Lead Nitrate. An Accurate, Sensitive Thermometer for Variable-Temperature MAS. *J. Magn. Reson. Ser. A* **1995**, *116*, 215–220.

(37) van Gorkom, L. C. M.; Hook, J. M.; Logan, M. B.; Hanna, J. V.; Wasylishen, R. E. Solid-State Lead-207 NMR of lead(II) Nitrate: Localized Heating Effects at High Magic Angle Spinning Speeds. *Magn. Reson. Chem.* **1995**, *33*, 791–795.

(38) Boulineau, S.; Courty, M.; Tarascon, J.-M.; Viallet, V. Mechanochemical Synthesis of Li-

Argyrodite Li_6PS_5X (X=Cl, Br, I) as Sulfur-Based Solid Electrolytes for All Solid State Batteries Application. *Solid State Ionics* **2012**, *221*, 1–5.

(39) Kotobuki, M.; Kanamura, K.; Sato, Y.; Yoshida, T. Fabrication of All-Solid-State Lithium Battery with Lithium Metal Anode Using Al_2O_3-Added $Li_7La_3Zr_2O_{12}$ Solid Electrolyte. *J. Power Sources* **2011**, *196*, 7750–7754.

(40) Feng, J. K.; Lu, L.; Lai, M. O. Lithium Storage Capability of Lithium Ion Conductor $Li_{1.5}Al_{0.5}Ge_{1.5}(PO_4)_3$. *J. Alloys Compd.* **2010**, *501*, 255–258.

(41) Seino, Y.; Takada, K.; Kim, B.-C.; Zhang, L.; Ohta, N.; Wada, H.; Osada, M.; Sasaki, T. Synthesis of Phosphorous Sulfide Solid Electrolyte and All-Solid-State Lithium Batteries with Graphite Electrode. *Solid State Ionics* **2005**, *176*, 2389–2393.

(42) Jain, A.; Ong, S. P.; Hautier, G.; Chen, W.; Richards, W. D.; Dacek, S.; Cholia, S.; Gunter, D.; Skinner, D.; Ceder, G.; et al. Commentary: The Materials Project: A Materials Genome Approach to Accelerating Materials Innovation. *APL Mater.* **2013**, *1*, 11002.

(43) Roos, A.; Schoonman, J. Electronic Conductivity in $La_{1-x}Ba_xF_{3-x}$ Crystals. *Solid State Ionics* **1984**, *13*, 205–211.

(44) Glassner, A. *The Thermochemical Properties of the Oxides, Fluorides, and Chlorides to 2500° K*; report ANL-5750, Argonne National Laboratory, Lemont, 1957.

(45) Bezmelnitsyn, V. N.; Bezmelnitsyn, A. V.; Kolmakov, A. A. New Solid-State Electrochemical Source of Pure Fluorine. *J. Fluor. Chem.* **1996**, *77*, 9–12.

(46) Badway, F.; Cosandey, F.; Pereira, N.; Amatucci, G. G. Carbon Metal Fluoride

Nanocomposites. *J. Electrochem. Soc.* **2003**, *150*, A1318.

(47) Hua, X.; Robert, R.; Du, L. S.; Wiaderek, K. M.; Leskes, M.; Chapman, K. W.; Chupas, P. J.; Grey, C. P. Comprehensive Study of the CuF_2 Conversion Reaction Mechanism in a Lithium Ion Battery. *J. Phys. Chem. C* **2014**, *118*, 15169–15184.

(48) Giraudet, J.; Dubois, M.; Hamwi, A.; Stone, W. E. E.; Pirotte, P.; Masin, F. Solid-State NMR (^{19}F and ^{13}C) Study of Graphite Monofluoride $(CF)_n$: ^{19}F Spin−Lattice Magnetic Relaxation and $^{19}F/^{13}C$ Distance Determination by Hartmann−Hahn Cross Polarization. *J. Phys. Chem. B* **2005**, *109*, 175–181.

(49) Leifer, N. D.; Johnson, V. S.; Ben-Ari, R.; Gan, H.; Lehnes, J. M.; Guo, R.; Lu, W.; Muffoletto, B. C.; Reddy, T.; Stallworth, P. E.; et al. Solid-State NMR Studies of Chemically Lithiated CF_x. *J. Electrochem. Soc.* **2010**, *157*, A148–A154.

(50) Vyalikh, A.; Bulusheva, L. G.; Chekhova, G. N.; Pinakov, D. V.; Okotrub, A. V.; Scheler, U. Fluorine Patterning in Room-Temperature Fluorinated Graphite Determined by Solid-State NMR and DFT. *J. Phys. Chem. C* **2013**, *117*, 7940–7948.

(51) Seid, K.-A.; Badot, J.-C.; Perca, C.; Dubrunfaut, O.; Soudan, P.; Guyomard, D.; Lestriez, B. An In Situ Multiscale Study of Ion and Electron Motion in a Lithium-Ion Battery Composite Electrode. *Adv. Energy Mater.* **2015**, *5*, 1400903.

(52) Han, F.; Zhu, Y.; He, X.; Mo, Y.; Wang, C. Electrochemical Stability of $Li_{10}GeP_2S_{12}$ and $Li_7La_3Zr_2O_{12}$ Solid Electrolytes. *Adv. Energy Mater.* **2016**, *6*, 1501590.

(53) Valerga, A. J.; Badachhape, R. B.; Parks, G. D.; Karmachik, P.; Wood, J. L.; Margrave, J.

L. *Thermodynamic and Kinetic Data of Carbon-Fluorine Compounds*; Report Rice University, Houston, 1974.

(54) Nakajima, T.; Watanabe, N. *Graphite Fluorides and Carbon-Fluorine Compounds*; CRC Press: Boca Raton, 1991.

Table of content: